doi:10.1038/nature13390

Modality-specific thalamocortical inputs instruct the identity of postsynaptic L4 neurons

Gabrielle Pouchelon[1], Frédéric Gambino[1]†, Camilla Bellone[1], Ludovic Telley[1], Ilaria Vitali[1], Christian Lüscher[1,2,3], Anthony Holtmaat[1] & Denis Jabaudon[1,2,3]

During development, thalamocortical (TC) input has a critical role in the spatial delineation and patterning of cortical areas[1–6], yet the underlying cellular and molecular mechanisms that drive cortical neuron differentiation are poorly understood. In the primary (S1) and secondary (S2) somatosensory cortex, layer 4 (L4) neurons receive mutually exclusive input originating from two thalamic nuclei[7,8]: the ventrobasalis (VB), which conveys tactile input[9,10], and the posterior nucleus (Po), which conveys modulatory and nociceptive input[11–14]. Recently, we have shown that L4 neuron identity is not fully committed postnatally[15], implying a capacity for TC input to influence differentiation during cortical circuit assembly. Here we investigate whether the cell-type-specific molecular and functional identity of L4 neurons is instructed by the origin of their TC input. Genetic ablation of the VB at birth resulted in an anatomical and functional rewiring of Po projections onto L4 neurons in S1. This induced acquisition of Po input led to a respecification of postsynaptic L4 neurons, which developed functional molecular features of Po-target neurons while repressing VB-target traits. Respecified L4 neurons were able to respond both to touch and to noxious stimuli, in sharp contrast to the normal segregation of these sensory modalities in distinct cortical circuits. These findings reveal a behaviourally relevant TC-input-type-specific control over the molecular and functional differentiation of postsynaptic L4 neurons and cognate intracortical circuits, which instructs the development of modality-specific neuronal and circuit properties during corticogenesis.

Within S1, VB axons target L4 neurons, forming cortical barrels, and Po axons target L5A and L1 neurons; in S2, however, Po axons target L4 neurons (Fig. 1a, b)[7,8,16,17]. Molecular distinctions between L4 neurons in S1 and S2, such as *Rorb* expression[18] (Fig. 1c), may therefore in part be driven by their distinct TC inputs. To investigate TC-type-specific controls over L4 neuron identity, we genetically ablated the VB at birth by generating transgenic *Slc6a4*::Cre/*Rosa26*::stop^{flox}*DTA* mice (*vb*$^{-}$ mice)[19,20], leading to death of VB neurons between postnatal day (P)0 and P4 and lack of formation of associated S1 whisker-mapped cortical barrels (Fig. 1d–h and Extended Data Figs 1, 2a–c). Remarkably, S1L4 remained richly innervated by TC terminals despite the absence of VB axons, as shown using the pan-TC presynaptic marker VGLUT2 (ref. 18) (Fig. 1i), without evidence for secondary cell death (Extended Data Fig. 2d–g). These terminals did not belong to residual VB axons, as they were still present at P23 (Extended Data Fig. 2b) and did not express the VB-specific markers 5HTT (5-hydroxytryptamine transporter) and GSBS (G-substrate)[21] (Fig. 1j, k). These data indicate that S1L4 neurons still receive TC input in the absence of VB.

To identify the origin of these ectopic TC projections, we retrogradely labelled TC neurons from S1, revealing that Po is the exclusive source of TC input to S1 in *vb*$^{-}$ mice (Extended Data Fig. 3a–f′). Po$_{vb-}$ neurons were undistinguishable from control Po neurons by microarray comparative gene expression analysis (Extended Data Fig. 3g), demonstrating that bona fide Po neurons are the source of S1L4 TC input in *vb*$^{-}$ mice. To directly visualize aberrant Po$_{vb-}$ projections, we next anterogradely

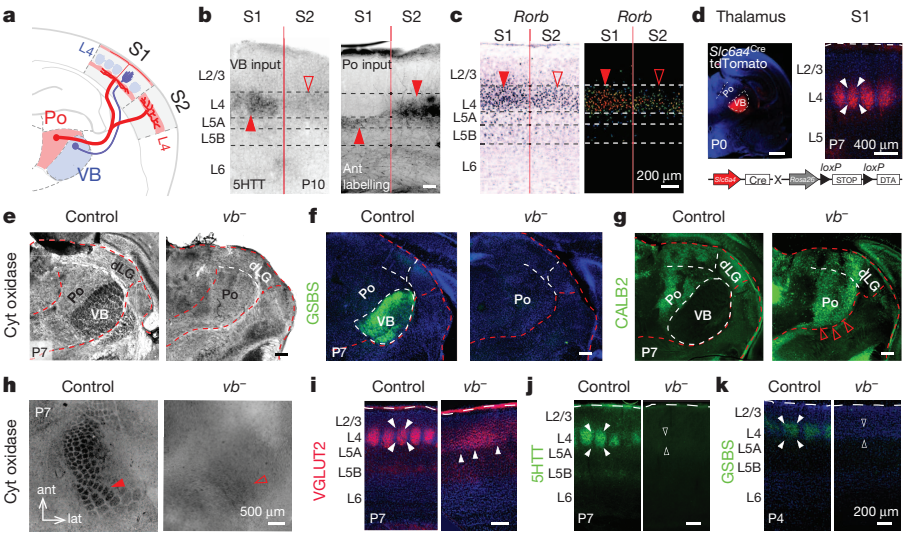

Figure 1 | TC input to S1L4 is preserved in *vb*$^{-}$ mice. a, **b**, VB and Po TC axons have specific projections to S1 and S2. **c**, *Rorb* expression is area-specific in L4 neurons (from Allen Brain Atlas). **d**, tdTomato reporter expression driven by *Slc6a4*^{Cre} shows VB-specific recombination. **e–h**, *vb*$^{-}$ mice lack VB (**e–g**) and lack presynaptic barrels in S1 (**h**). Ant, anterograde; Cyt oxidase, cytochrome oxidase; dLG, dorsolateral geniculate nucleus. **i**, Presynaptic TC terminals are still present in S1$_{vb-}$ cortex using the pan-TC presynaptic marker VGLUT2. **j**, **k**, VB-specific presynaptic markers are lacking in S1$_{vb-}$.

[1]Department of Basic Neurosciences, Faculty of Medicine, University of Geneva, CH-1211 Geneva, Switzerland. [2]Clinic of Neurology, Department of Clinical Neurosciences, Geneva University Hospital, CH-1211 Geneva, Switzerland. [3]Institute of Genetics & Genomics in Geneva (iGE3), University of Geneva, CH-1211 Geneva, Switzerland. †Present address: Interdisciplinary Institute for NeuroScience, CNRS UMR 5297, 33077 Bordeaux, France.

labelled Po and VB axons in control mice and Po axons in vb^- mice. Control VB axons branched within S1L4 and Po axons were excluded from this layer, whereas conversely, in S2, where VB axons were not found, Po axons branched within L4 (Fig. 2a, b, d). By contrast, in $S1_{vb-}$, Po neurons projected densely to L4 (Fig. 2c, d; $P < 0.05$ for Po control (Po_{Ctrl}) versus Po_{vb-} axonal length in L4, Student's *t*-test, $n = 3$ control and $n = 4$ vb^- labellings). Po axons formed functional synapses onto $S1L4_{vb-}$ neurons, as demonstrated by short-latency synaptic responses to optogenetic stimulation of these axons, which were absent in control S1L4 barrel neurons (Fig. 2e, f). By contrast, Po-S2L4 connectivity was unchanged in vb^- cortex (Extended Data Fig. 3h, i), and Po rewiring in S1 was not observed following focal VB ablation at P10 (Supplementary Note 1). Taken together, these results indicate that Po axons substitute for VB axons in vb^- mice, providing a new source of presynaptic input to L4 neurons.

We next investigated whether this VB→Po switch in TC input instructs cell-type-specific developmental gene expression programs in postsynaptic L4 neurons. We first characterized the molecular identity of wild-type cortical neurons in L2/3, L4, and L5/6 of S1 and S2 using microarray analysis of microdissected samples[22] at P10 (Fig. 3a, b and Extended Data Fig. 4a, b). The genetic relatedness between these samples was determined using unbiased cluster analysis, revealing three classes of transcriptional programs: L2/3-like, L4-like and L5/6-like. Analysis of $S1L4_{vb-}$ samples revealed an L4-like transcriptional program, demonstrating that TC input origin does not determine the laminar molecular identity of L4 neurons (Fig. 3c).

We next investigated whether TC input origin instructs distinct differentiation programs in VB-receiving (S1L4) and Po-receiving (S2L4) neurons. To examine whether the VB→Po switch in TC input repressed VB-target and induced Po-target differentiation programs, we first defined S1L4- and S2L4-type transcripts by identifying wild-type L4-specific genes whose expression was mutually exclusive between S1 and S2 (Fig. 3d). Analysis of the expression of these two gene sets by $S1L4_{vb-}$ neurons revealed a strong repression of S1L4-type genes and a corresponding induction of S2L4-type genes (Fig. 3e–g; $P < 0.0001$ for S1L4 ($n = 74$ genes) and <0.005 for S2L4 ($n = 74$ genes) percentage expression level, paired Student's *t*-test). This respecification of molecular identity was further examined using *in situ* hybridization for select gene candidates including the S1L4-type transcript *Rorb*, which was strongly decreased in $S1L4_{vb-}$ neurons, and the S2L4-type transcript *Cdh8*, which was upregulated (Fig. 3h, i and Extended Data Fig. 4c–e). VB input-dependent changes in S1L4 gene expression coincided with the postnatal maturation of VB-L4 synapses, and failed to occur in $S1L4_{vb-}$ neurons, resulting in an S2L4-type developmental gene expression program (Extended Data Figs 1a–i, 5 and Supplementary Note 2).

We next investigated the respective contribution of VB input loss and Po input acquisition to these genetic changes. Comparison of vb^- mice

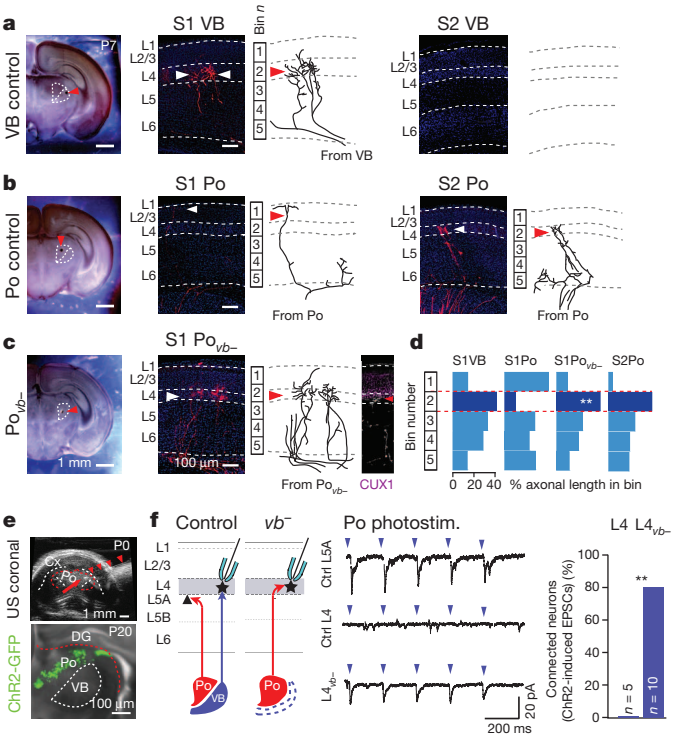

Figure 2 | Po TC axons are rewired onto S1L4 neurons in vb^- mice. **a**, **b**, Anterograde labelling in control mice showing arborization of VB axons within S1L4 (**a**, left) and exclusion of Po axons from this layer (**b**, left). In S2, VB axons are absent (**a**, right) whereas Po axons arborize in S2L4 (**b**, right). **c**, Po_{vb-} axons arborize within S1L4. **d**, Quantification. $^{**}P < 0.005$, Student's *t*-test, $n = 3$ control (Ctrl) and $n = 4$ vb^- injections. **e**, Ultrasound (US)-guided microinjection of a AAV-ChR2-GFP virus into Po. Red arrowheads indicate location of the micropipette shaft. **f**, Optogenetic stimulation of Po axons elicits excitatory postsynaptic currents (EPSCs) in S1L5A neurons but not S1L4 neurons, whereas EPSCs are evoked in $S1L4_{vb-}$ neurons. $^{**}P < 0.005$, Student's *t*-test.

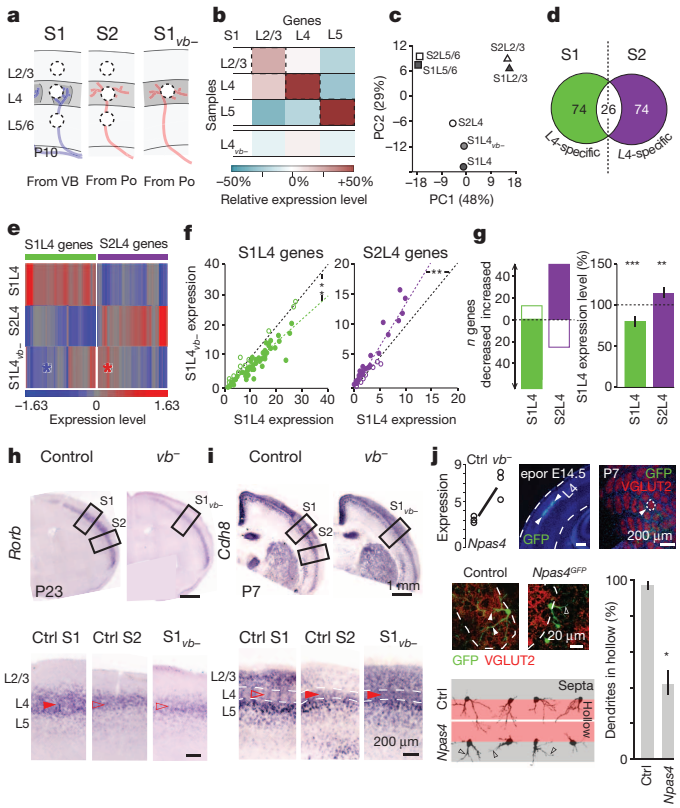

Figure 3 | VB→Po switch in input congruently respecifies $S1L4_{vb-}$ neurons. **a**, Schematic experimental design. **b**, Validation of sample collection with known marker genes for L2/3, L4 and L5/6 neurons (see ref. 22 and Methods). **c**, Principal component (PC) analysis plot of sample-specific gene expression showing clustering of L2/3 (triangles), L4 (circles) and L5/6 (squares) transcriptional programs. **d**, Delineation of S1L4-type and S2L4-type transcripts. **e**, Heatmap representation showing repression of a subset of S1L4-type genes (blue asterisk) and induction of S2L4-type genes (red asterisk) in $L4_{vb-}$ neurons. **f**, Levels of expression of S1L4-type genes (green: full, decreased; open, increased) and S2L4-type genes (purple: full, increased; open, decreased) in $L4_{vb-}$ neurons. $^{**}P < 10^{-4}$, Student's *t*-test. **g**, 62 out of 74 S1L4-type genes are downregulated in $S1L4_{vb-}$ neurons; 50 out of 74 S2L4-type genes are upregulated in $S1L4_{vb-}$ neurons. $^{***}P < 10^{-5}$, $^{**}P < 0.005$, paired Student's *t*-test; $n = 74$ S1L4-type and 74 S2L4-type genes. **h**, **i**, *In situ* hybridization illustrating cell-type-specific downregulation of *Rorb* (**h**), and upregulation of *Cdh8* (**i**). **j**, Overexpression of an *Npas4*^{GFP}-expressing construct into S1L4 neurons disrupts the polarization of dendrites towards barrel hollows (that is, VB axon-containing barrel centres) at P7. $^{*}P < 0.05$, $n = 19$ Ctrl and $n = 10$ *Npas4*$^+$ neurons, ANOVA. Error bars denote mean ± s.e.m.

with *Dlx5/6*::Cre/*Celsr3*^{flox} mice, which entirely lack TC input[23], revealed that each input type instructs the differentiation program of S1L4$_{vb-}$ neurons, as some genes were strictly VB-input-dependent, whereas others were Po-input-dependent (Extended Data Fig. 6 and Supplementary Note 3). Together, these data indicate that VB and Po axons exert input-type-specific controls over S1L4 neuron genetic identity.

We next examined the functional role of the top input-dependent S1L4 transcripts, which together formed a core set of genes involved in neurite differentiation and polarization (Extended Data Table 1). The transcription factors *Npas4* (ref. 24) and *Zbtb20* (ref. 25) and the extracellular protein *Sema3a* (ref. 26) were functionally characterized using *in vitro* and *in vivo* morphological analysis of embryonic day (E)14.5-electroporated L4 neurons. Each of these transcripts controlled neurite polarization *in vitro* and postnatal orientation of S1L4 neuron primary dendrites towards VB axons *in vivo*, a key requisite for columnar assembly of cortical circuits (Fig. 3j, Extended Data Fig. 7 and Supplementary Note 4). Thus, VB input exerts a genetic control over the development of critical morphological circuit-related properties of S1L4 neurons.

To further investigate the role of VB input in intracortical circuit assembly, we determined excitatory/inhibitory (E/I) feed-forward responses of L4 neurons to optogenetic stimulation of VB (for S1L4 neurons) and Po axons (for S2L4 and S1L4$_{vb-}$, Extended Data Fig. 8a). Supporting a TC-type-specific control over intracortical circuit assembly, S1L4$_{vb-}$ E/I responses were increased to S2L4 levels (Extended Data Fig. 8b–d; $P < 0.05$ for S1L4 versus S2L4 and S1L4 versus S1L4$_{vb-}$; $P = 0.4$ for S2L4 versus S1L4$_{vb-}$, analysis of variance (ANOVA), $n = 5$ Ctrl, 7 S2L4 and 6 S1L4$_{vb-}$ neurons). VB→Po switch in input thus instructs corresponding downstream changes in intracortical circuit properties.

As VB neurons normally transmit tactile information[9,10] and Po neurons nociceptive information[12–14], we examined whether the VB→Po switch in input led to a congruent shift in the functional identity of S1L4 neurons (Fig. 4a). The trigeminal principalis nucleus (PrV), which provides input to VB, was notably atrophied in *vb*$^-$ mice, whereas Po afferent pathways remained unchanged, suggesting that the locus of the plasticity in *vb*$^-$ mice is essentially thalamocortical (Extended Data Fig. 9 and Supplementary Note 5). In control mice, single-whisker environmental exploration led to activation of S1L4 neurons in the corresponding barrel, as reported by expression of the immediate-early gene *c-fos* (also known as *Fos*)[14,27] (Fig. 4b). S1L4$_{vb-}$ neurons were also activated by this task, although more diffusely, consistent with the broader distribution of presynaptic Po$_{vb-}$ terminals and S2-like increases in S1L4$_{vb-}$ E/I responses (Supplementary Note 6). Back-and-forth deflections of single whiskers in head-fixed mice evoked focal intrinsic optical signal responses in S1 (Fig. 4c)[28], which were weaker and more variable than in control mice, suggesting asynchronous cortical activation. Accordingly, *in vivo* intracellular recordings revealed a ~3-fold increase in the jitter of L2/3-evoked responses to whisker deflections and prolonged onset latencies in *vb*$^-$ mice (Fig. 4d, $P < 0.05$ for jitter and latency, Mann–Whitney rank-sum test, $n = 7$ Ctrl and 6 *vb*$^-$ cells). Consistent with this degradation in the coding of input signals, *vb*$^-$ mice were distinctly impaired at tasks requiring haptic skills and fine sensorimotor coordination (Fig. 4e and Supplementary Note 7). Together, these findings reflect the low fidelity of spatial and temporal encoding in Po ascending pathways[29] and indicate that Po-input-receiving S1L4$_{vb-}$ neurons still respond, albeit less reliably, to tactile stimuli *in vivo*.

To investigate whether respecified S1L4$_{vb-}$ neurons acquired the ability to respond to noxious stimuli, we performed a microinjection of capsaicin, an algogenic chemical, into the whisker pad of *vb*$^-$ mice[14]. In control mice, S1L5A neurons and S2L4 neurons were strongly activated, as revealed by c-Fos expression, while S1L4 neurons remained inactive, reflecting the normal target specificity of Po projections[14]. By contrast, S1L4$_{vb-}$ neurons were activated by noxious stimulation, in a pattern similar to that of S2L4 of control mice (Fig. 4f; $P < 0.001$ for L4 versus L4$_{vb-}$, Student's *t*-test; $n = 3$ Ctrl and $n = 3$ *vb*$^-$ mice). Consistent with an expanded L4 population response to Po input, *vb*$^-$ mice displayed increased behavioural signs of pain following capsaicin injection and shortened flick latencies to focal thermic tail stimulation (Supplementary Videos 1 and 2, Fig. 4g and Supplementary Note 7). Taken together, these data indicate that rewiring of Po input onto VB targets results in an abnormal convergence of normally segregated tactile and nociceptive sensory modalities onto S1L4 neurons.

Our findings reveal that distinct TC inputs exert modality-specific controls over the molecular identity and function of postsynaptic L4 neurons. VB and Po inputs only affected a specific subset of S1L4- and

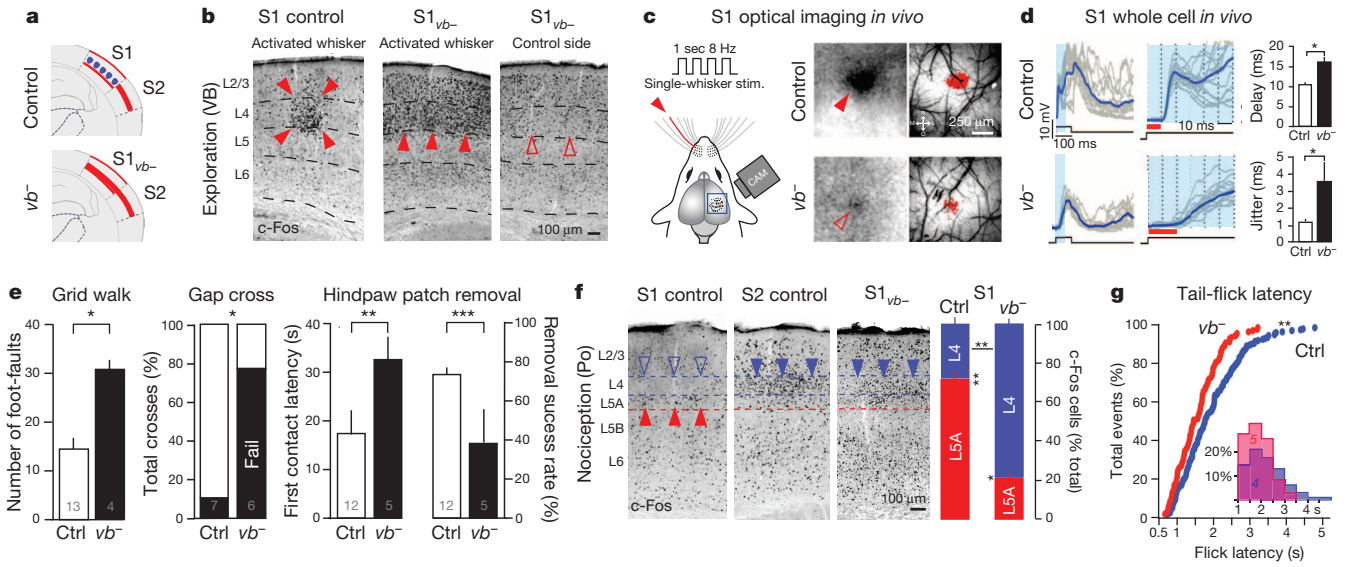

Figure 4 | Functional convergence of normally segregated sensory modalities in *vb*$^-$ mice. a, S1L4$_{vb-}$ neurons acquire S2L4-type functional properties. **b**, S1L4$_{vb-}$ neurons are activated during environmental exploration. **c**, Single-whisker stimulation elicits weak focal S1 responses in *vb*$^-$ mice. **d**, EPSCs from sample L2/3 neurons. Delay and increased jitter of responses to whisker deflections in *vb*$^-$ mice (*$P < 0.05$, Mann–Whitney rank-sum test, $n = 7$ Ctrl and 6 *vb*$^-$ neurons). **e**, Haptic skills and fine sensorimotor coordination are impaired in *vb*$^-$ mice (see Supplementary Note 7). *$P < 0.05$, **$P = 0.008$, ***$P < 0.0005$, Student's *t*-test. **f**, Noxious stimulation of the whisker-pad activates S1L4$_{vb-}$ neurons but not S1L4 neurons ($n = 3$ Ctrl and $n = 3$ *vb*$^-$ mice; *$P < 0.05$, ** $P < 0.005$, Student's *t*-test) (L4 versus L5A in *vb*$^-$ mice, $P < 0.01$; L4 versus L5A in control mice, $P < 0.005$; L4 versus L4$_{vb-}$, $P < 0.005$). **g**, *vb*$^-$ mice have shorter flick latencies upon focal thermic stimulation of the tail. ** $P < 0.005$, Kolmogorov–Smirnov test. Error bars denote mean ± s.e.m.

S2L4-type genes, such that the identity of S1L4$_{vb-}$ neurons was intermediate between these two neuronal types. This intermediate genetic identity is reminiscent of the cytoarchitectonically 'hybrid' visual cortex found following *in utero* bilateral enucleation in monkeys[30], suggesting that input-type-dependent specification may have contributed to cortical neuron diversity during evolution.

Po-dependent 'non-lemniscal' somatosensory pathways are thought to be evolutionary older than VB-dependent 'lemniscal' pathways (see ref. 14 and references therein). Emergence of a specialized VB-dependent pathway during evolution suggests that VB axons were at competitive advantage over pre-existing Po axons. Supporting this possibility, our findings reveal that Po axons invade VB targets in *vb*$^-$ cortex, and VB and Po axons co-mingle in the early postnatal cortex before segregating into their anatomically complementary patterns[16]. Therefore, evolutionary and developmental segregation of tactile and nociceptive pathways may have occurred via hierarchical interactions between VB and Po inputs.

Finally, the circuit-specific transcriptional controls described here provide a powerful mechanism matching terminal neuronal differentiation to specific functional constraints. Whereas cell-intrinsic differentiation programs initially define neuronal permissiveness to distinct inputs[15], reciprocally, these inputs differentially instruct gene expression programs in their targets. This crosstalk between gene expression and circuit connectivity may therefore act to orchestrate the assembly of cognate neurons into functionally specialized pathways during development.

METHODS SUMMARY

Animals. Compound mice were generated as described in Methods.
Histology. Brains were fixed and stained using standard methods[14,15].
Anterograde and retrograde labelling. Retrograde cortical labelling was performed using stereotaxic FluoroGold microinjections. Anterograde cortical labelling was performed on fixed brains using NeuroVue Dye Filter Red (MTTI, FS-1002) inserted into the VB or the Po.
Microdissection and microarray analysis. L2/3, L4 and L5/6 in S1 and S2 of P10 controls and *vb*$^-$ mice were microdissected. After amplification and labelling of extracted RNA, hybridization onto Affymetrix Mouse Gene 1.0 ST arrays was performed.
ChR2 injections and electrophysiology. A ChR2-Venus-expressing adenovirus (AAV5-hSyn-hChR2 H134R) was used. Electrophysiology recordings were performed at 3 weeks of age[15].
***In utero* electroporations.** These were performed as described in ref. 15.
Tactile and noxious stimulations. These were performed as detailed in ref. 14.
***In vivo* electrophysiology.** Intrinsic imaging and whole-cell recordings were performed as detailed in ref. 28.
Behavioural tests. These were performed as described in the Methods.

Online Content Any additional Methods, Extended Data display items and Source Data are available in the online version of the paper; references unique to these sections appear only in the online paper.

Received 11 October 2013; accepted 22 April 2014.
Published online 14 May 2014.

1. Sur, M., Garraghty, P. E. & Roe, A. W. Experimentally induced visual projections into auditory thalamus and cortex. *Science* **242,** 1437–1441 (1988).
2. Dehay, C., Horsburgh, G., Berland, M., Killackey, H. & Kennedy, H. Maturation and connectivity of the visual cortex in monkey is altered by prenatal removal of retinal input. *Nature* **337,** 265–267 (1989).
3. Katz, L. C. & Shatz, C. J. Synaptic activity and the construction of cortical circuits. *Science* **274,** 1133–1138 (1996).
4. Miyashita-Lin, E. M., Hevner, R. F., Wassarman, K. M., Martinez, S. & Rubenstein, J. L. R. Early neocortical regionalization in the absence of thalamic innervation. *Science* **285,** 906–909 (1999).
5. Chou, S.-J. *et al.* Geniculocortical input drives genetic distinctions between primary and higher-order visual areas. *Science* **340,** 1239–1242 (2013).
6. Li, H. *et al.* Laminar and columnar development of barrel cortex relies on thalamocortical neurotransmission. *Neuron* **79,** 970–986 (2013).
7. Wimmer, V. C., Bruno, R. M., de Kock, C. P. J., Kuner, T. & Sakmann, B. Dimensions of a projection column and architecture of VPM and POm axons in rat vibrissal cortex. *Cereb. Cortex* **20,** 2265–2276 (2010).
8. Ohno, S. *et al.* A morphological analysis of thalamocortical axon fibers of rat posterior thalamic nuclei: a single neuron tracing study with viral vectors. *Cereb. Cortex* **22,** 2840–2857 (2012).
9. Nicolelis, M. A. L. Computing with thalamocortical ensembles during different behavioural states. *J. Physiol. (Lond.)* **566,** 37–47 (2005).
10. Yu, C., Derdikman, D., Haidarliu, S. & Ahissar, E. Parallel thalamic pathways for whisking and touch signals in the rat. *PLoS Biol.* **4,** e124 (2006).
11. Ahissar, E., Sosnik, R. & Haidarliu, S. Transformation from temporal to rate coding in a somatosensory thalamocortical pathway. *Nature* **406,** 302–306 (2000).
12. Gauriau, C. & Bernard, J.-F. Posterior triangular thalamic neurons convey nociceptive messages to the secondary somatosensory and insular cortices in the rat. *J. Neurosci.* **24,** 752–761 (2004).
13. Masri, R. *et al.* Zona incerta: a role in central pain. *J. Neurophysiol.* **102,** 181–191 (2009).
14. Frangeul, L. *et al.* Specific activation of the paralemniscal pathway during nociception. *Eur. J. Neurosci.* http://dx.doi.org/10.1111/ejn.12524 (2 March 2014).
15. De la Rossa, A. *et al. In vivo* reprogramming of circuit connectivity in postmitotic neocortical neurons. *Nature Neurosci.* **16,** 193–200 (2013).
16. Kichula, E. A. & Huntley, G. W. Developmental and comparative aspects of posterior medial thalamocortical innervation of the barrel cortex in mice and rats. *J. Comp. Neurol.* **509,** 239–258 (2008).
17. Viaene, A. N., Petrof, I. & Sherman, S. M. Properties of the thalamic projection from the posterior medial nucleus to primary and secondary somatosensory cortices in the mouse. *Proc. Natl Acad. Sci. USA* **108,** 18156–18161 (2011).
18. Jabaudon, D., Shnider, S. J., Tischfield, D. J., Galazo, M. J. & Macklis, J. D. *RORβ* induces barrel-like neuronal clusters in the developing neocortex. *Cereb. Cortex* **22,** 996–1006 (2012).
19. Narboux-Nême, N., Pavone, L. M., Avallone, L., Zhuang, X. & Gaspar, P. Serotonin transporter transgenic (SERTcre) mouse line reveals developmental targets of serotonin specific reuptake inhibitors (SSRIs). *Neuropharmacology* **55,** 994–1005 (2008).
20. Brockschnieder, D. *et al.* Cell depletion due to diphtheria toxin fragment A after Cre-mediated recombination. *Mol. Cell. Biol.* **24,** 7636–7642 (2004).
21. Endo, S. G-substrate: the cerebellum and beyond. *Prog. Mol. Biol. Transl. Sci.* **106,** 381–416 (2012).
22. Belgard, T. G. *et al.* A transcriptomic atlas of mouse neocortical layers. *Neuron* **71,** 605–616 (2011).
23. Zhou, L. *et al.* Early forebrain wiring: genetic dissection using conditional Celsr3 mutant mice. *Science* **320,** 946–949 (2008).
24. Yun, J. *et al.* Neuronal Per Arnt Sim (PAS) domain protein 4 (NPAS4) regulates neurite outgrowth and phosphorylation of synapsin I. *J. Biol. Chem.* **288,** 2655–2664 (2013).
25. Nielsen, J. V., Blom, J. B., Noraberg, J. & Jensen, N. A. Zbtb20-induced CA1 pyramidal neuron development and area enlargement in the cerebral midline cortex of mice. *Cereb. Cortex* **20,** 1904–1914 (2010).
26. Shelly, M. *et al.* Semaphorin3A regulates neuronal polarization by suppressing axon formation and promoting dendrite growth. *Neuron* **71,** 433–446 (2011).
27. Wagener, R. J., Dávid, C., Zhao, S., Haas, C. A. & Staiger, J. F. The somatosensory cortex of reeler mutant mice shows absent layering but intact formation and behavioral activation of columnar somatotopic maps. *J. Neurosci.* **30,** 15700–15709 (2010).
28. Gambino, F. & Holtmaat, A. Spike-timing-dependent potentiation of sensory surround in the somatosensory cortex is facilitated by deprivation-mediated disinhibition. *Neuron* **75,** 490–502 (2012).
29. Sosnik, R., Haidarliu, S. & Ahissar, E. Temporal frequency of whisker movement. I. Representations in brain stem and thalamus. *J. Neurophysiol.* **86,** 339–353 (2001).
30. Rakic, P., Suñer, I. & Williams, R. W. A novel cytoarchitectonic area induced experimentally within the primate visual cortex. *Proc. Natl Acad. Sci. USA* **88,** 2083–2087 (1991).

Supplementary Information is available in the online version of the paper.

Acknowledgements We thank S. Endo for the gift of the G-substrate antibody, N. Aagaard Jensen for the gift of the *miR-Zbtb20* construct, F. Ango for the gift of the *Sema3a*-Tomato construct, and A. Goffinet for the gift of *Dlx5/6*::Cre/*Celsr3*^{flox} tissue. We are thankful to A. Benoit and F. Smets for technical assistance, to B. Golding for help with the *in situ* hybridizations, to O. Schaad, C. Barraclough and M. Docquier of the Genomics Platform of the University of Geneva for help with the microarray experiments. We thank E. Azim and F. Rijli for their comments on the manuscript. Work in the Jabaudon laboratory is supported by the Swiss National Science Foundation (SNF) (PP00P3_123447), the Leenaards Foundation, the Synapsis Foundation and the NARSAD Foundation. C.B. was supported by an Ambizione grant from the SNF and by the Gertrude von Meissner Foundation, C.L. by the SNF and the Simons Foundation Autism Research Initiative (SFARI), and F.C. and A.H. by the SNF (grant 31003A-135631), EMBO, the International Foundation for Research in Paraplegia, and the Hans Wilsdorf Foundation.

Author Contributions D.J. and G.P. conceived the project, D.J. and C.B. designed the electrophysiological experiments, and G.P., C.B., I.V., L.T., F.G. and D.J. performed the experiments. D.J. and G.P. wrote the manuscript with help from C.L. and A.H.

Author Information Reprints and permissions information is available at www.nature.com/reprints. The authors declare no competing financial interests. Readers are welcome to comment on the online version of the paper. Correspondence and requests for materials should be addressed to D.J. (denis.jabaudon@unige.ch).

METHODS

Mice. C57BL/6 and CD1 mice, *Slc6a4*^{Cre} transgenic mice[31], Ai14 transgenic reporter mice (Jackson Laboratories, stock number 007914)[32] and Rosa26::stop^{flox}*DTA*[20] males and females were used. Experiments were carried out in accordance with the Institutional Animal Care and Use Committee of the University of Geneva and with permission of the Geneva cantonal authorities.

Histology. Postnatal mice were perfused with 4% paraformaldehyde (PFA) and brains were fixed overnight in 4% PFA at 4 °C. 50-μm vibratome sections (Leica VT1000S) were used for all histological experiments. S1L4 and S2L4 neurons were visually identified on the basis of tangential location using topographical atlases (S1 versus S2) and bin location (L4 = bins 3–4 out of 10, see Extended Data Fig. 2f, g).

In situ hybridization on slides was performed according to methods described previously[33]. In brief, hybridization was carried out overnight at 60 °C with the digoxigenin (DIG)-labelled RNA probes. After hybridization, sections were washed and incubated with alkaline phosphatase-conjugated anti-DIG antibody (Roche 1:2,000) overnight at 4 °C. After incubation, sections were washed and the colour reaction was carried out overnight at 4 °C in a solution containing NBT (nitro-blue tetrazolium chloride) and BCIP (5-bromo-4-chloro-3′-indoly phosphate *p*-toluidine salt) (Roche). After colour revelation, sections were washed, post-fixed for 30 min in 4% PFA and mounted with Fluromount (Sigma). For antisense probe synthesis, total complementary DNA was amplified by PCR with primers designed for specific messenger RNA sequence of *Pcdh20*, *NeuroD6* and *Grm4*. T7 or Sp6 promoter sequence was added to the reverse primer sequence. DIG-labelled antisense RNA probes were obtained after *in vitro* transcription of the resulted PCR product (Roche kit) or of the plasmid template for *Rorb* and *Cdh8* (kind gift from M. Studer).

For immunohistochemistry, brain sections were incubated 1 h at room temperature in a blocking solution containing 3% BSA and 0.3% Triton X-100 in PBS and incubated overnight at 4 °C with primary antibodies: rabbit anti-5HTT (1/500, Calbiochem, PC177L), rabbit anti-GSBS (1/2,000, gift from S. Endo)[21], rabbit anti-CALB2 (1/500, Swant, 7699/3H), guinea pig anti-VGLUT2 (1/2,000, Millipore, AB2251), mouse anti-GFAP (1/500, Sigma, G3893), rabbit anti-c-Fos (1/5,000, Santa Cruz, sc-52), rabbit anti-CUX1 (1:200, Santa Cruz, sc-13024). Sections were rinsed three times in PBS and incubated for 60–90 min at room temperature with the Alexa Fluor 488- or 546-conjugated secondary antibodies (1/500, Invitrogen). For c-Fos immunostaining, biotinylated goat secondary anti-rabbit antibody (1/200, Invitrogen) were used, followed by an amplification step with Vectastain ABC kit (Vector Laboratories) and revealed in a 0.05% DAB, 0.02% $NiSO_4$, 0.025% $CoCl_2$ and 0.01% H_2O_2 solution. DAPI (0.2 μg ml^{-1}) was used for fluorescent nuclear counterstaining.

For Nissl staining, brain sections were mounted, stained with 0.5% cresyl violet and dehydrated with graded alcohols. For cytochrome oxidase staining: free-floating sections were placed in a solution of 0.5 mg ml^{-1} DAB, 0.5 mg ml^{-1} cytochrome C (Sigma), 40 mg ml^{-1} sucrose, 0.1 mM Tris, pH 7.6 at 37 °C until staining appears. Fluoro-Jade B staining was performed as previously described[34] with Fluoro-Jade B kit (Millipore).

Imaging and quantifications. All photomicrographs were taken with an Eclipse 90i fluorescence microscope (Nikon, Japan) or with a LSM700 confocal microscope (Zeiss). Where cells were counted, this was performed on a minimum of three biological replicates, within a 0.25 mm^2 area encompassing the whole radial extent of the cortex, and divided into 5 or 10 bins. Photomicrographs are representative examples taken from ≥2 replicates.

Anterograde/retrograde labelling. Focal retrograde labelling from the cortex: anaesthetized P7 mice were placed on a stereotaxic apparatus thalamic neurons were retrogradely labelled via 55-nl injections of FluoroGold (FG) 2% (Hydroxystilbamidine bis(methanesulphonate), Fluorochrome Inc.). Brains were collected 2 days after the injection. Focal retrograde labelling from the Po (Extended Data Fig. 9d): 92 nl of Alexa Fluor 555-conjugated cholera toxin subunit B (Invitrogen) was microinjected stereotactically at P10 and brains were collected at P23 and sectioned coronally. Only injections confined to the Po were analysed ($n = 4$ Ctrl and $n = 3$ vb^- injections).

For anterograde labelling, the caudal part of fixed P7 brains was cut to reveal the caudal thalamus. Trypan blue staining was applied to allow distinction between thalamic nuclei and anterograde labelling was initiated by insertion of small NeuroVue Dye-coated Filter Red (MTTI, FS-1002) (50 × 50 μm^2) in VB or Po. Brains were incubated at 37 °C in 0.4% PFA for 8 weeks and cut into 100-μm sections on a vibratome before immediate imaging. TC layer-specific arborization was quantified by measuring axonal length within each of the 5 bins using ImageJ software. Analysis was performed on 3–5 100-μm-thick sections corresponding to bregma levels −0.82 to −1.58 on the Paxinos adult brain atlas; S1 analyses were performed in the cortex at the same dorsolateral level as the hippocampus, whereas S2 was identified as the region lateral to this, adjacent to the piriform cortex.

Tissue microdissection and microarray. One mouse of control and vb^- littermates were used to collect each of three biological replicates of L2/3, L4, L5/6 samples at P10 for cortical microarrays, or of Po and VB for thalamic microarrays. Fresh coronal brain sections (140 μm) were cut on a vibrating microtome and thalamic nuclei or cortical layers were visually identified and microdissected using a Leica Stereomicroscope (Leica M165FC) in ice-cold oxygenated artificial cerebrospinal fluid under RNase-free conditions. Samples were stored in RNAlater at −80 °C. RNA was extracted using an RNeasy kit (Qiagen) and one- or two-cycle amplification and labelling was performed (according to Affymetrix protocols) using Superscript cDNA synthesis kit (Invitrogen), MEGAscript T7 kit and MessageAmp IIaRNA amplification kit (Ambion). Labelled cRNA was fragmented and hybridized to Affymetrix Mouse Gene 1.0 ST arrays (for cortical samples) or mouse 430 2.0 Genome arrays (for thalamic samples). GeneChips were incubated at 45 °C for 16 h with biotin-labelled cRNA probes, and then washed and stained using a streptavidin-phycoerythrin conjugate with antibody amplification as described in Affymetrix protocol, using Affymetrix GeneChip Fluidics Station 450. GeneChips were scanned on a GCS3000 scanner (Affymetrix).

Microarray CEL files were normalized using Robust Multichip Analysis and analysed using Partek Genomics Suites software (http://www.partek.com). The accuracy of the microdissection approach was validated by measuring concordance of gene expression of the samples with genes confirmed to be strongly enriched in one cortical layer. Relative gene expression = (expression in the defined layer – mean expression in all layers)/(mean expression in all layers)[22]. We defined the laminar identity of L4, L2/3 and L5/6 neurons within S1 and S2 by using ANOVA (fold change >2; $P < 0.05$, adjusted for multiple comparisons within Partek Genomic Suites) to identify their top 100 most specifically expressed genes in each of the six collected control samples. The relatedness between these six samples and $L4_{vb-}$ was determined using unbiased cluster analysis of this reference set of genes (total 600 transcripts, of which 453 are unique).

***In utero* electroporation and tissue culture.** E14.5 timed pregnant CD1 mice were anaesthetized with isoflurane/oxygen and a pCAG-*GFP* reporter plasmid or CMV-*SEMA3A-Tomato*[35] (kind gift from F. Ango), pCAG-*Npas4-GFP* (Thermo Fisher Scientific, MMM1013-202733015) or pCAG-miR*Zbtb20-GFP*[25] (kind gift from N. A. Jensen) construct was injected into the embryos' lateral ventricle using a 40-μm-tip glass micropipette mounted on a Nanoject II nanoinjector (Drummond Scientific). E14.5 was chosen as a gestational age to specifically target L4 neuron progenitors[15]. Voltage pulses (40 mV, 50 ms) were applied using external paddles in order to target S1, as described previously[15]. Females were allowed to give birth and P7 pups were fixed with intracardiac perfusion of 4% PFA. Tangential sections of flattened electroporated cortex were cut at 50 μm and immunostaining for VGLUT2 was performed. Images were taken at LSM700 Zeiss confocal. The delineation between barrel septae and hollows was performed on serially reconstructed image stacks using the ImageJ software. The total number of primary dendrites and distribution of dendrites within hollows or septae were determined and statistically analysed using an ANOVA test across conditions.

For *in vitro* culture, electroporated mouse embryos were dissected at E16.5 in ice-cold HBSS. The S1-positive electroporated site was microdissected under fluorescent microscopy and dissociated cells cultured during 3 days on 12-mm, coated coverslips (poly-L-lysine, 0.1 mg ml^{-1}) in 500 μl Neurobasal supplemented with GlutaMAX, B27, sodium pyruvate and a mixture of antibiotic penicillin-streptomycin all from Gibco. The cultures were then fixed with 4% PFA, mounted with DAPI and analysed on a LSM 700 Zeiss confocal and ImageJ software.

***In vitro* electrophysiology.** AAV-mediated expression of ChR2 (AAV5-hsynhChR2 H134R) was injected at P0 in the Po, under ultrasound guidance (Vevo 660, VisualSonics). Injected mice were collected 3 weeks later and processed for electrophysiology. ~P23 mice were deeply anaesthetized with isoflurane and were then decapitated. Brains were removed and placed in cold (0–4 °C), oxygenated (95% O_2–5% CO_2) slicing solution containing: 119 mM NaCl, 2.5 mM KCl, 1.3 mM MgCl, 2.5 mM $CaCl_2$, 1.0 mM Na_2HPO_4, 26.2 mM $NaHCO_3$ and 11 mM glucose. Coronal slices (300 mM) were kept at room temperature and were allowed to recover for at least 1 h before recording. Under low magnification, the barrels in L4 could be readily identified, and high-power magnification was used to guide the recording electrode onto visually identified neurons. The radial extent of the cortex was virtually divided into 5 bins (1 = most pial) and patched neurons were always located in bin 2, which corresponds to L4, as validated in pilot experiments in which neurons were filled with biocytin (3 mg ml^{-1}) for 15 min and location was assessed using immunostaining of CUX1 after fixing fresh sections ($n = 7$ Ctrl and $n = 6$ vb^-) in both S1 and S2. The internal solution contained 140 mM potassium gluconate, 5 mM KCl, 10 mM HEPES, 0.2 mM EGTA, 2 mM $MgCl_2$, 4 mM Na_2ATP, 0.3 mM Na_3GTP and 10 mM sodium creatine-phosphate. Currents were amplified (Multiclamp 700B, Axon Instruments), filtered at 5 kHz and digitized at 20 kHz (National Instruments Board PCI-MIO-16E4, Igor, WaveMetrics). The liquid junction potential was +12 mV. Experiments were discarded if the access resistance varied by more than 20%. Synaptic currents were evoked by light flashes delivered by a fibre optic cable (Thorlabs) attached to a 473-mm solid-state laser (CrystaLaser). Cells were held at −60 mV and GABA currents were blocked by wash in picrotoxin

(Tocris, 100 μM). Light-evoked EPSCs were recorded at −46 mV and light-evoked IPSCs were recorded at 0 mV (ref. 36) (Extended Data Fig. 8).

***In vivo* electrophysiology**

Intrinsic optical imaging. ~P23 mice were first anaesthetized with isoflurane (4% for induction with ~0.5 l min^{-1} O_2), and then with urethane (1.5 g kg^{-1}, i.p., prepared in lactated ringer solution containing in mM: 102 NaCl, 28 Na L-Lactate, 4 KCl, 1.5 $CaCl_2$). Eye ointment was applied to prevent dehydration. The scalp was locally anaesthetized with lidocaine (1%), the periosteum gently removed, and a custom-made plastic chamber was attached to the skull above barrel cortex (centred 1.5–2 mm posterior from bregma, 2–2.5 mm lateral) with dental acrylic and dental cement. The chamber was filled with sterile cortex buffer (containing in mM: 125 NaCl, 5 KCl, 10 glucose, 10 HEPES, 2 $CaCl_2$, and 2 $MgSO_4$, pH 7.4) and sealed with a glass coverslip. Intrinsic optical signals were imaged through the intact skull using an Imager 3001F[28].

***In vivo* whole-cell patch clamp.** After imaging, a small, ~1 × 1 mm piece of bone was removed using a dental drill (centred above the C2 whisker maximum intrinsic optical signal response). Whole-cell 'blind' patch-clamp recordings were obtained as previously described[28]. High positive pressure (200–300 mbar) was applied to the pipette (7–9 MΩ) to prevent tip occlusion while penetrating the dura. After passing the dura the positive pressure was immediately reduced to prevent cortical damage. The pipette was then advanced in 2-μm steps, and pipette resistance was monitored in the conventional voltage-clamp configuration. When the pipette resistance suddenly increased, positive pressure was relieved to obtain a 3–5-GΩ seal. After break-in, the membrane potential (V_m) was measured, and dialysis was allowed to occur for at least 5 min before deflecting the whisker. Data were acquired using a Multiclamp700B amplifier (Molecular Devices), and digitized at 10 kHz (National Instruments), using MATLAB (Mathworks)-based Ephus software (http://research.janelia.org/labs/display/ephus; The Janelia Farm Research Center). Off-line analysis was performed using custom routines written in IgorPro (Wavemetrics). All neurons were located at ~200 μm below the pia.

Current-clamp recordings were made using a potassium-based internal solution (in mM: 135 potassium gluconate, 4 KCl, 10 HEPES, 10 Na_2-phosphocreatine, 4 Mg-ATP, 0.3 Na-GTP, pH adjusted to 7.25 with KOH, 285 mOsm). Series resistance (R_s) and input resistance (R_{in}, not including R_s) were monitored with a 100-ms long-lasting hyperpolarizing square pulse 400 ms before each whisker deflection, and extracted off-line by using a double exponential fit. Recordings were discarded if one of the following conditions occurred: (1) V_m and R_s exceeded −50 mV and 50 MΩ, respectively; (2) spontaneously occurring spikes were not overshooting; (3) R_s or R_{in} changed more than 30% over the duration of the experiment. The bridge was usually not balanced and liquid junction potential was not corrected.

Whisker-evoked post-synaptic potential (PSP) analysis. Whisker-evoked PSPs were evoked by forth and back deflection of the whisker (100 ms, 0.1 Hz) using piezoelectric ceramic elements attached to a glass pipette ~4 mm away from the skin. The voltage applied to the ceramic was set to evoke a whisker displacement of ~0.6 mm with a ramp of 7–8 ms. The C1 and C2 whiskers were independently deflected by different piezoelectric elements. PSP analyses were confined to down states. Peak amplitude and integral analysis was performed on each trace, and then presented as a mean of at least 30 whisker-evoked responses. The PSP onset latency was defined as the time point at which the amplitude exceeded 3 × s.d. of the baseline noise over 5 ms before stimulation. The jitter was defined as the standard deviation of at least 30 whisker-evoked responses (control mice, $n = 7$ cells per 3 mice; vb^- mice, $n = 6$ cells per 3 mice).

Environmental enrichment. All but one whisker (C1) on the right side of the snout were clipped in P23 vb^- or control mice ($n = 3$), after which the animals were placed in an large playground box containing plastic balls, maze-like pieces of thread, and various small objects, as previously described. Mice were kept for 1 h in enriched environment, perfused and brains stained for c-Fos expression[14,27,37].

Noxious stimulation. P23 vb^- or control mice were briefly anaesthetized with isoflurane, and 50 μl of a capsaicin solution (10 mM (Sigma), 100% ethanol and 7% Tween-80 in saline) was subcutaneously injected in the whisker pad as previously described[14,38]. Mice were allowed to wake up and were euthanized after 1 h and their brain stained for c-Fos expression. The number of c-Fos^+ neurons was quantified on five sections per animal ($n = 3$) in a ~600-μm width of S1 (~3 barrels). Statistical comparisons of layer-specific c-Fos activation between control and vb^- mice were done using Student's *t*-test.

Behavioural analysis. ~P30 vb^- mice and littermates were used for all behavioural experiments. Both males and females were used. To habituate animals to the testing environment, mice were transported within their home cage to the testing room for three consecutive days before testing. All behavioural tests took place during the light phase of the light–dark cycle, with the observer blinded to the mouse genotype.

For the open field test, spontaneous locomotor activity was examined in $n = 6$ vb^- mice and $n = 17$ control littermates. Mice were placed in the centre of a 45 × 45-cm arena and locomotion in the dark (distance travelled, percentage time spent in central, intermediate or lateral sectors) was recorded during 15 min using an infrared camera coupled to a tracking software (ANYmaze, Stoelting Co). For the grid-walk test, sensorimotor abilities (limb placement accuracy, coordination) of hindlimbs were examined in $n = 4$ vb^- mice and $n = 13$ control littermates by assessing the aptitude of the mice to navigate in dim lighting over a wire mesh grid (2.4 × 2.4-cm grid spaces, 45 × 45-cm total area) during 6 min[39,40]. Foot-faults were counted when a hindlimb paw protruded entirely through the grid. For the gap-crossing test, whisker-sensing abilities and sensorimotor coordination were examined in $n = 7$ vb^- mice and $n = 6$ control littermates by placing mice on a 12 × 12 cm elevated platform and measuring the number of crosses performed to a neighbouring platform across a 4-cm gap in obscurity. The gap was such that the mouse was required to extend its head and detect the opposite platform with its whiskers before crossing[41,42]. The number of crosses and failed attempts (that is, falls) were recorded by an observer via an infrared camera. A maximum of two falls per mouse was admitted after which the test was interrupted. Adhesive patch removal task: this test was originally developed to assess somatosensory asymmetry and sensory function after sensorimotor cortex lesions[43–45]. $n = 5$ vb^- mice and $n = 12$ control littermates were used. A 6-mm diameter circular adhesive patch was placed on the plantar surface of each hindpaw, after which mice were released in the testing arena and observed for 240 s. Latency to detect the first patch (snout contact with the patch) as well as the time taken to remove both patches was measured. Mice underwent three consecutive trials, with an inter-trial interval of 60 min, and values were averaged for each mouse. For the tail-flick test, sensitivity to noxious stimuli was determined using the tail-flick test[46] in $n = 5$ vb^- mice and $n = 4$ control littermates. In the apparatus (IITC Life Science), a pre-focused light beam supplied an area of 4 × 6-mm heat stimulation to the tail. The time taken for the mouse to flick its tail away from the stimulation area was recorded, providing a measure of pain sensitivity. Values were obtained from three sessions of ten trials (inter-session interval: 24 h).

Statistics. No statistics were used to determine group sample size; however, sample sizes were similar to those used in previous publications from our group and others. The person performing the test was blinded to the animal's genotype. All mice were used in the study; the tail-flick test was performed only if the animal collaborated to rest with its tail in the flick detection groove. If animals undertook more than one task, the order of the task was randomized. Two-tailed *t*-tests were used for all statistical analyses except for the tail-flick test, for which values had a non-Gaussian distribution, which was analysed using a Kolmogorov–Smirnov test. Values are shown as mean ± s.e.m. throughout the manuscript. *n* values refer to biological replicates throughout the manuscript.

31. Zhuang, X., Masson, J., Gingrich, J. A., Rayport, S. & Hen, R. Targeted gene expression in dopamine and serotonin neurons of the mouse brain. *J. Neurosci. Methods* **143,** 27–32 (2005).
32. Madisen, L. *et al.* A robust and high-throughput Cre reporting and characterization system for the whole mouse brain. *Nature Neurosci.* **13,** 133–140 (2010).
33. Lai, T. *et al.* SOX5 controls the sequential generation of distinct corticofugal neuron subtypes. *Neuron* **57,** 232–247 (2008).
34. Schmued, L. C. & Hopkins, K. J. Fluoro-Jade B: a high affinity fluorescent marker for the localization of neuronal degeneration. *Brain Res.* **874,** 123–130 (2000).
35. Cioni, J.-M. *et al.* SEMA3A signaling controls layer-specific interneuron branching in the cerebellum. *Curr. Biol.* **23,** 850–861 (2013).
36. Gabernet, L., Jadhav, S. P., Feldman, D. E., Carandini, M. & Scanziani, M. Somatosensory integration controlled by dynamic thalamocortical feed-forward inhibition. *Neuron* **48,** 315–327 (2005).
37. Bisler, S. *et al.* Expression of c-Fos, ICER, Krox-24 and JunB in the whisker-to-barrel pathway of rats: time course of induction upon whisker stimulation by tactile exploration of an enriched environment. *J. Chem. Neuroanat.* **23,** 187–198 (2002).
38. Noma, N. *et al.* Organization of pERK-immunoreactive cells in trigeminal spinal nucleus caudalis and upper cervical cord following capsaicin injection into oral and craniofacial regions in rats. *J. Comp. Neurol.* **507,** 1428–1440 (2008).
39. Z'Graggen, W. J., Metz, G. A., Kartje, G. L., Thallmair, M. & Schwab, M. E. Functional recovery and enhanced corticofugal plasticity after unilateral pyramidal tract lesion and blockade of myelin-associated neurite growth inhibitors in adult rats. *J. Neurosci.* **18,** 4744–4757 (1998).
40. Leingärtner, A. *et al.* Cortical area size dictates performance at modality-specific behaviors. *Proc. Natl Acad. Sci. USA* **104,** 4153–4158 (2007).
41. Hutson, K. A. & Masterton, R. B. The sensory contribution of a single vibrissa's cortical barrel. *J. Neurophysiol.* **56,** 1196–1223 (1986).
42. Jenkinson, E. W. & Glickstein, M. Whiskers, barrels, and cortical efferent pathways in gap crossing by rats. *J. Neurophysiol.* **84,** 1781–1789 (2000).
43. Hernandez, T. D. & Schallert, T. Seizures and recovery from experimental brain damage. *Exp. Neurol.* **102,** 318–324 (1988).
44. Thallmair, M. *et al.* Neurite growth inhibitors restrict plasticity and functional recovery following corticospinal tract lesions. *Nature Neurosci.* **1,** 124–131 (1998).
45. Tomassy, G. S. *et al.* Area-specific temporal control of corticospinal motor neuron differentiation by COUP-TFI. *Proc. Natl Acad. Sci. USA* **107,** 3576–3581 (2010).
46. Le Bars, D., Gozariu, M. & Cadden, S. W. Animal models of nociception. *Pharmacol. Rev.* **53,** 597–652 (2001).

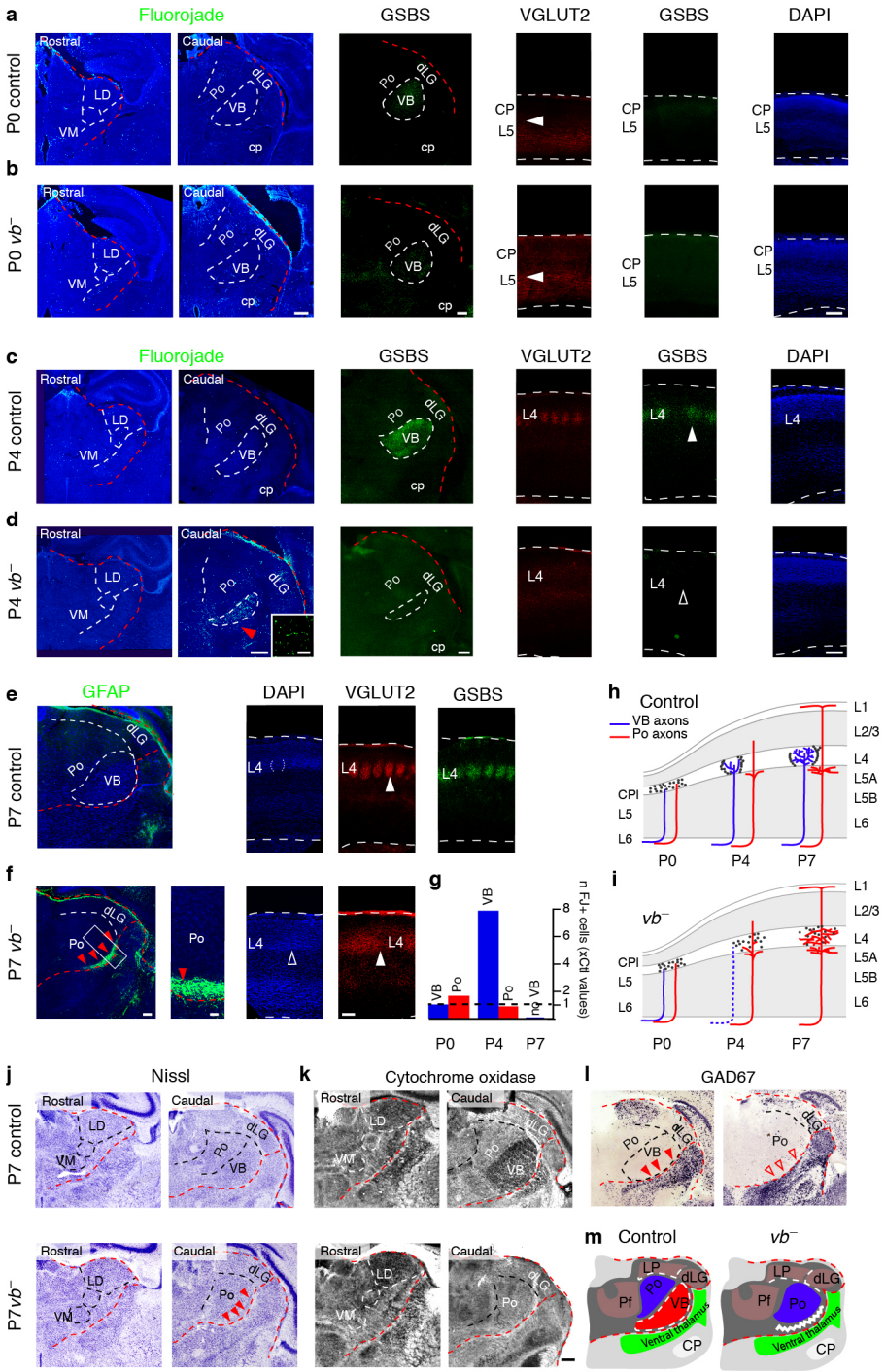

Extended Data Figure 1 | Early postnatal VB ablation in *vb*⁻ mice. **a**–**f**, Coronal sections of the thalamus and S1 cortex at P0 (**a**, **b**), P4 (**c**, **d**) and P7 (**e**, **f**) in control (**a**, **c**, **e**) and *vb*⁻ (**b**, **d**, **f**) mice. Staining for Fluoro-Jade B (FJ) reveals a peak of VB-specific neuronal degeneration at P4 in *vb*⁻ mice, a time at which the VB-specific marker GSBS[21] is already lacking. VGLUT2 immunostaining indicates that TC axons are present in deep cortical layers of *vb*⁻ mice at P0 (arrowhead) and reach L4 at P4, a time at which VB degeneration is at its peak. These axons are not clustered into whisker-related barrels and do not express the VB-specific marker GSBS, which is normally expressed at P4. DAPI (4′,6-diamidino-2-phenylindole) staining indicates that postsynaptic L4 neurons fail to assemble into barrels in *vb*⁻ cortex. At P7, immunostaining for the glial marker GFAP shows a secondary glial 'scar' (red arrowheads) at the ventral thalamic border in *vb*⁻ mice (**e**, **f**). **g**, Quantification of FJ⁺ neurons. **h**, **i**, Schematic representation of VB (blue) and Po (red) axonal development in control (**h**) and *vb*⁻ (**i**) S1 cortex. **j**, **k**, Nissl (**j**) and cytochrome oxidase (**k**) stainings reveal specific ablation of the VB in *vb*⁻ mice. **l**, *In situ* hybridization for the interneuron marker GAD67 shows preserved delineation of the dorsal and the ventral thalamus (red arrowheads). **m**, Schematic representation of *vb*⁻ thalamus. Scale bars, 200 μm (insets, 50 μm). CP, cerebral peduncle; CP, cortical plate; dLG, dorsolateral geniculate nucleus; LD, laterodorsal nucleus; LP, lateroposterior nucleus; PF, parafascicular nucleus; VM, ventromedial nucleus.

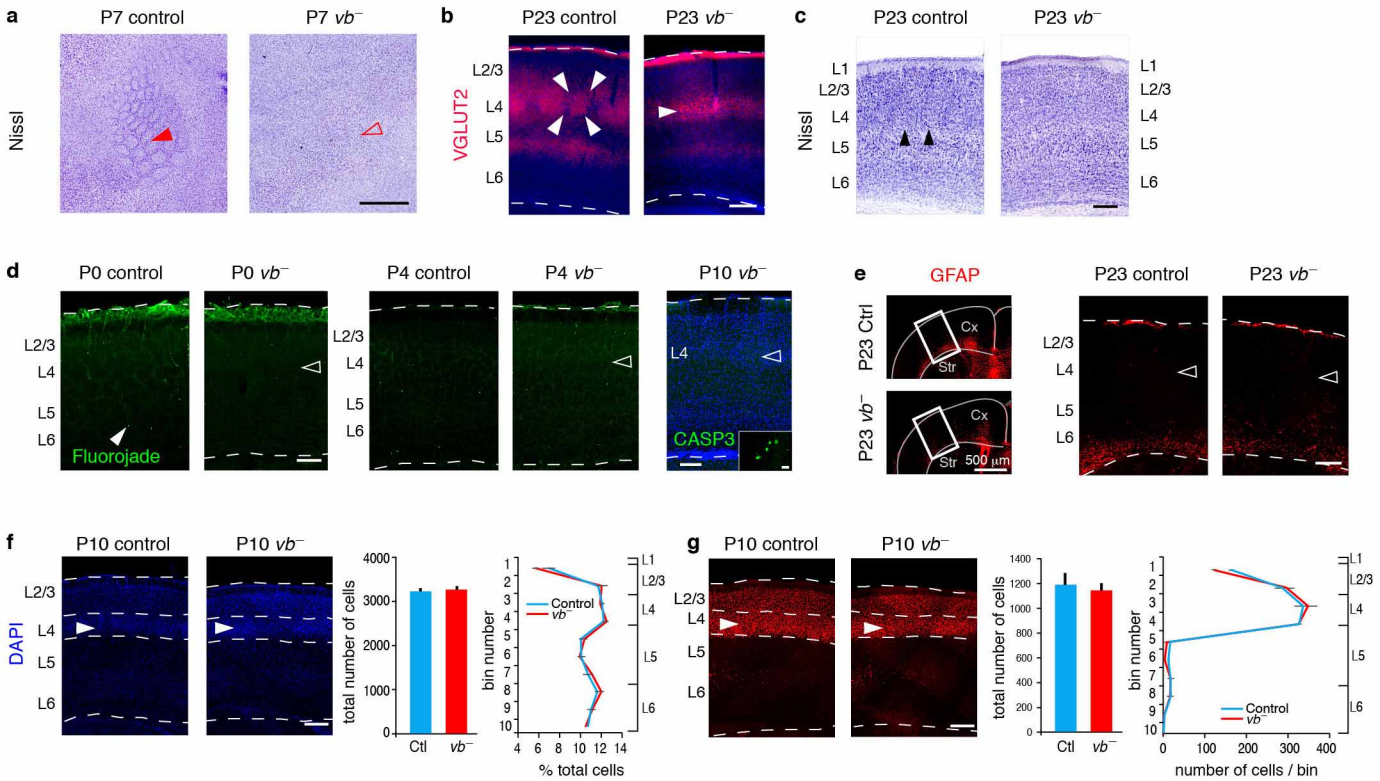

Extended Data Figure 2 | Rewiring of input to S1L4 occurs in the absence of cortical neuron death. **a**, Nissl-stained flattened preparation of the somatosensory cortex showing lack of barrel-like clusters in postsynaptic L4 cortical neurons in *vb*$^-$ mice (empty red arrowhead). **b**, **c**, Presynaptic TC terminals are still present in L4 of *vb*$^-$ cortex at P23 using the pan-TC presynaptic marker VGLUT2 (white arrowheads) (**b**) whereas cortical barrels are lacking (**c**). **d**, **e**, Fluoro-Jade B, cleaved caspase 3 (CASP3) (**d**) and GFAP (**e**) expression do not show evidence of cortical neuron degeneration in *vb*$^-$ mice (inset shows non-cortical CASP3$^+$ neurons in a non-cortical region of the same section). **f**, **g**, Staining and quantification using DAPI (**f**) and the L2/3-L4 marker CUX1 (**g**) show lack of barrels but preservation of S1L4 cell numbers in *vb*$^-$ mice. Total quantification surface: 0.25 mm^2. Scale bars, 400 µm (**a**), 200 µm (**b**–**d**, **f**, **g**), inset 10 µm (**d**).

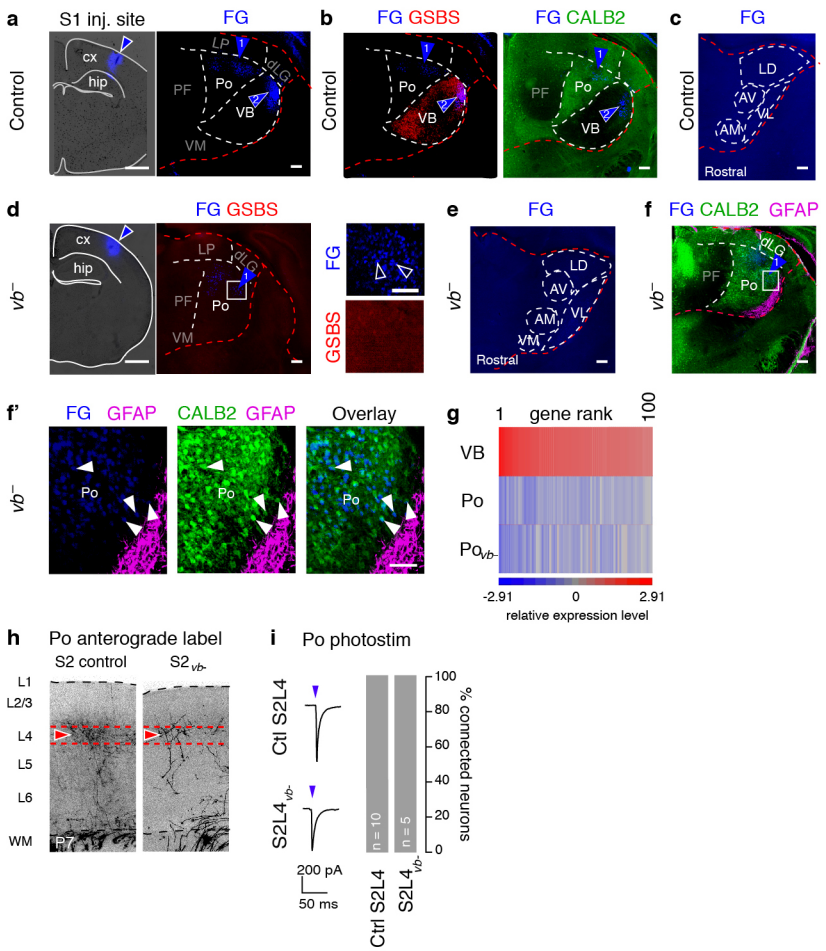

Extended Data Figure 3 | Ectopic TC projections to S1 in *vb*$^{-}$ mice originate from the Po. **a**–**c**, In control mice, retrograde labelling from S1 using FluoroGold (FG) labels both GSBS^{+} VB neurons and CALB2^{+} Po neurons (**b**, numbered blue arrowheads), whereas other thalamic nuclei are not detectably labelled (**b**, **c**). **d**–**f'**, In *vb*$^{-}$ mice, retrograde labelling from S1 exclusively labels GSBS^{-} Po neurons (**d**, blue arrowhead). No additional labelling is found in other thalamic nuclei (**d**, **e**). FG^{+} Po neurons are CALB2^{+} and located outside of the glial scar (**f**, **f'**: high magnification from inset in **f**). **g**, Po$_{vb-}$ neurons were undistinguishable from control Po neurons by molecular and microarray comparative gene expression analysis between Po$_{vb-}$, Po and VB neurons demonstrating that they are bona fide Po neurons. Heatmap representation of the expression intensity of the 100 most VB-specific genes in VB, Po and Po$_{vb-}$ neurons. None of these genes are statistically significantly upregulated in Po$_{vb-}$ neurons compared to Po. **h**, **i**, Po-S2L4 connectivity is normal in *vb*$^{-}$ as assessed by anterograde labelling of Po projections in S2L4$_{vb-}$ cortex (**h**) and S2L4 neuron responses to optogenetic stimulation of Po axons (**i**). Scale bars, 1 mm (low-magnification images) (**a**–**f**) and 100 µm elsewhere. AM, anteromedial; AV, anteroventral; Cx, cortex; dLG, dorsolateral geniculate; Hip, hippocampus; LD, laterodorsal; LP, lateroposterior; PF, parafascicular; VL, ventrolateral; VM, ventromedial.

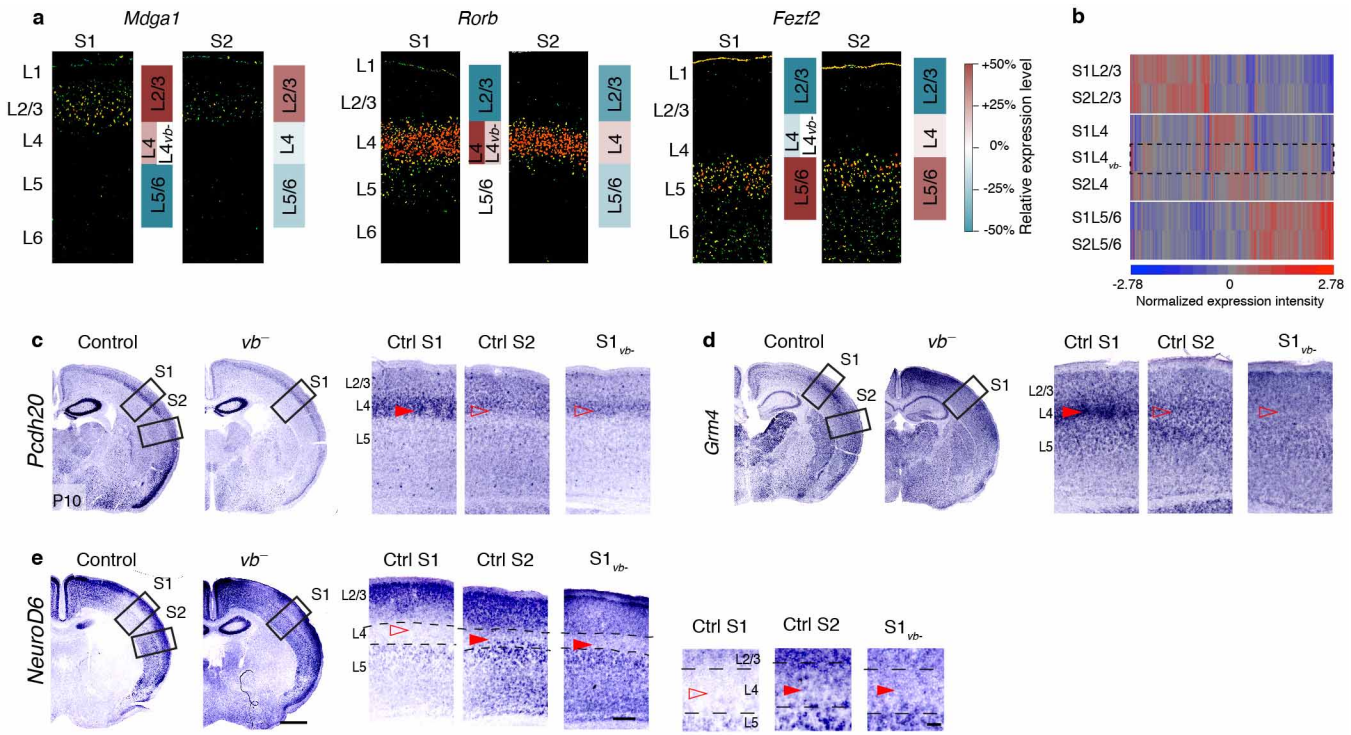

Extended Data Figure 4 | VB→Po switch in input leads to downregulation of S1L4 transcripts and upregulation of S2L4 transcripts in S1L4$_{vb-}$ neurons. **a**, *In situ* hybridizations (expression density map) from the Allen Brain Atlas (ABA) database showing expression of three sample genes specifically expressed in L2/3, L4 and L5 (*Mdga1*, *Rorb*, *Fezf2*, respectively). The heatmap on the right represents relative expression intensity in the microarray samples, which is concordant with the ABA data. Relative expression = (expression in the defined region – mean expression in all layers)/(mean expression in all layers) (see ref. 22). **b**, Heatmap representing sample-specific gene expression for the union of the top 100 most specifically expressed genes of L4$_{vb-}$, L2/3, L4 and L5/6 samples in S1 and S2. Note that S1L4$_{vb-}$ gene expression is intermediate between S1L4 and S2L4 neurons. **c**–**e**, *In situ* hybridization showing downregulation of the S1L4-enriched transcripts *Pcdh20* (**c**) and *Grm4* (**d**), and upregulation of S2L4-enriched transcripts *NeuroD6* (**e**) in S1L4$_{vb-}$ neurons. Scale bars, 1 mm (low magnifications), 100 μm (high magnifications), 30 μm (inset).

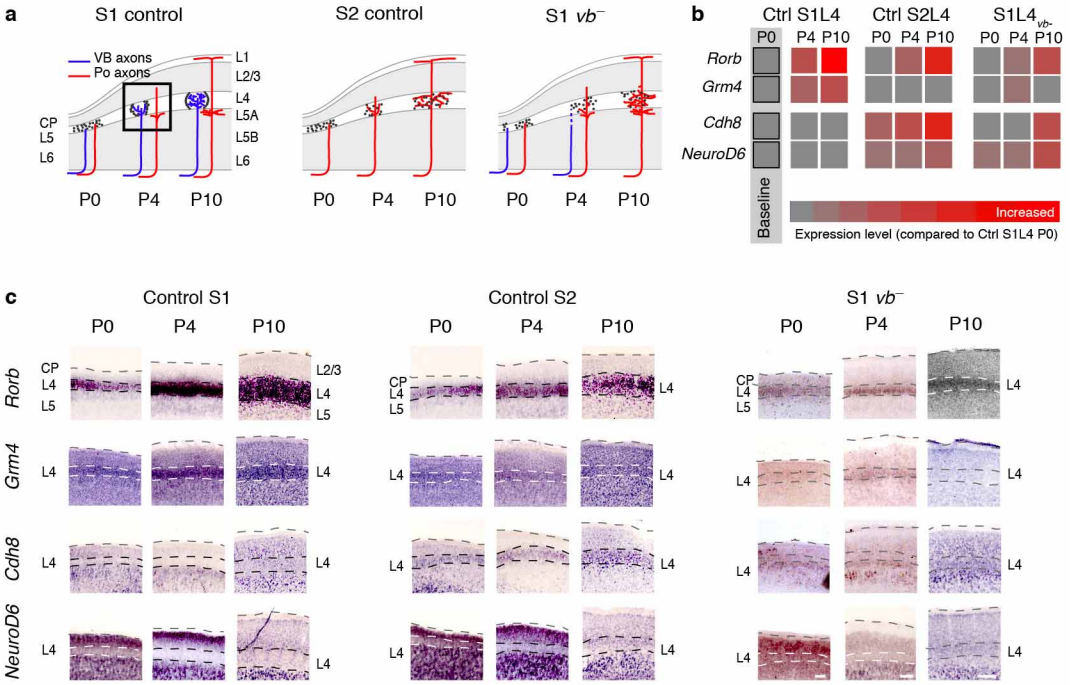

Extended Data Figure 5 | S1L4$_{vb-}$ developmental gene expression is S2L4-like. **a**, Schematic representation of VB (blue) and Po (red) axonal development in control S1 (left), control S2 (middle) and S1$_{vb-}$ (right) cortex. Boxed area indicates region shown in **c**. **b**, Summary of the findings: the time course of expression of L4 gene expression in S1L4$_{vb-}$ neurons is similar to that of S2L4 control cortex. Values are colour-coded using S1L4 P0 control values as baseline. **c**, *In situ* hybridizations for *Rorb* and *Grm4* (S1L4-type) and *Cdh8* and *NeuroD6* (S2-L4-type) transcripts at P0, P4 and P10 indicate that S1L4$_{vb-}$ developmental gene expression is S2L4-like. Scale bars, 100 µm. CP, cortical plate. See also Supplementary Note 2.

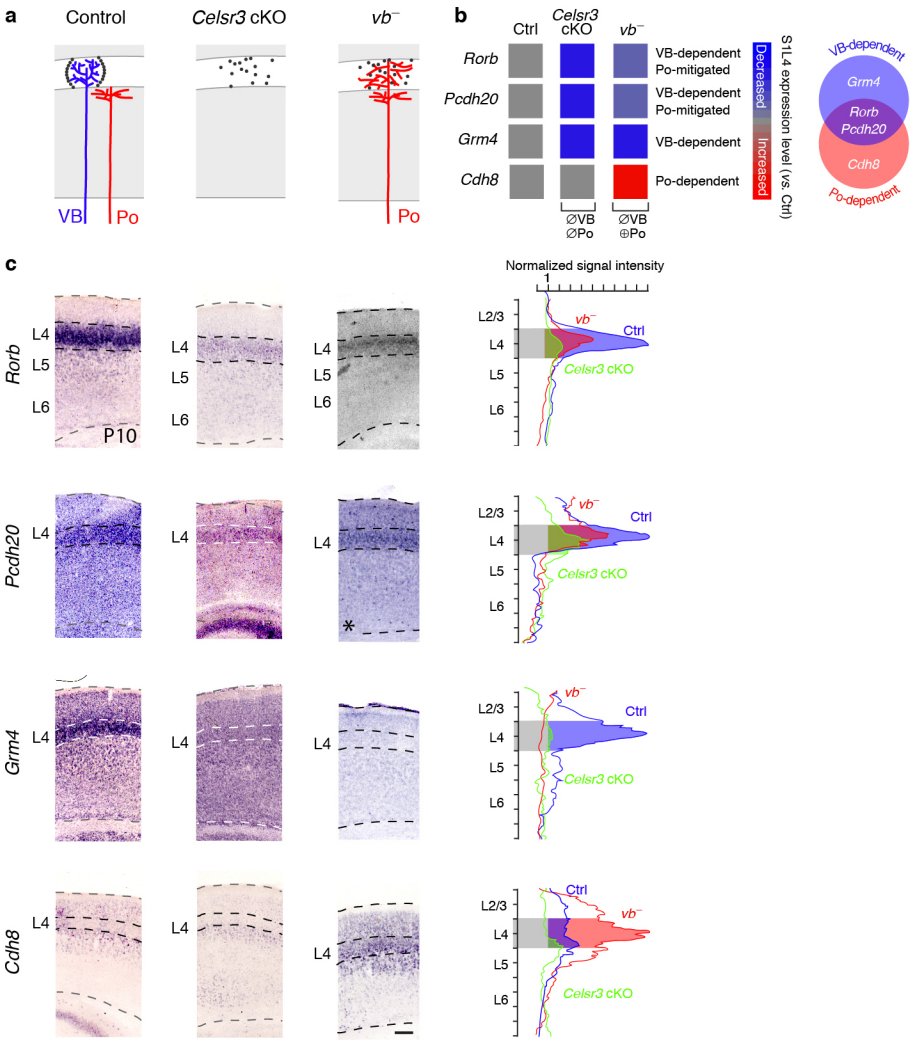

Extended Data Figure 6 | Loss of VB input and acquisition of Po input each define genetic changes in S1L4$_{vb-}$ neurons. a, Schematic representation of the phenotypes examined. *Celsr3* conditional knockouts (cKO) S1L4 neurons lack both VB and Po inputs (see Supplementary Note 3) whereas S1L4$_{vb-}$ receive Po but not VB input. **b**, Summary of the findings: expression of *Rorb* and *Pcdh20* expression is decreased both in *Celsr3* cKO and *vb*$^{-}$ L4 neurons, but this decrease is mitigated by Po input in *vb*$^{-}$ cortex. By contrast, *Grm4* expression is not rescued by Po input and is thus VB-dependent. *Cdh8* upregulation in *vb*$^{-}$ L4 neurons depends on Po input as it does not occur in the absence of TC input (*Celsr3* cKO). **c**, *In situ* hybridizations showing expression of the S1L4-type genes *Rorb*, *Pcdh20* and *Grm4*, and the S2L4-type gene *Cdh8*. The two photomicrographs with an asterisk are also presented in Extended Data Fig. 4. Normalized intensity values were obtained by radial scanning of intensity using the gel tool of ImageJ software. Scale bars, 200 μm.

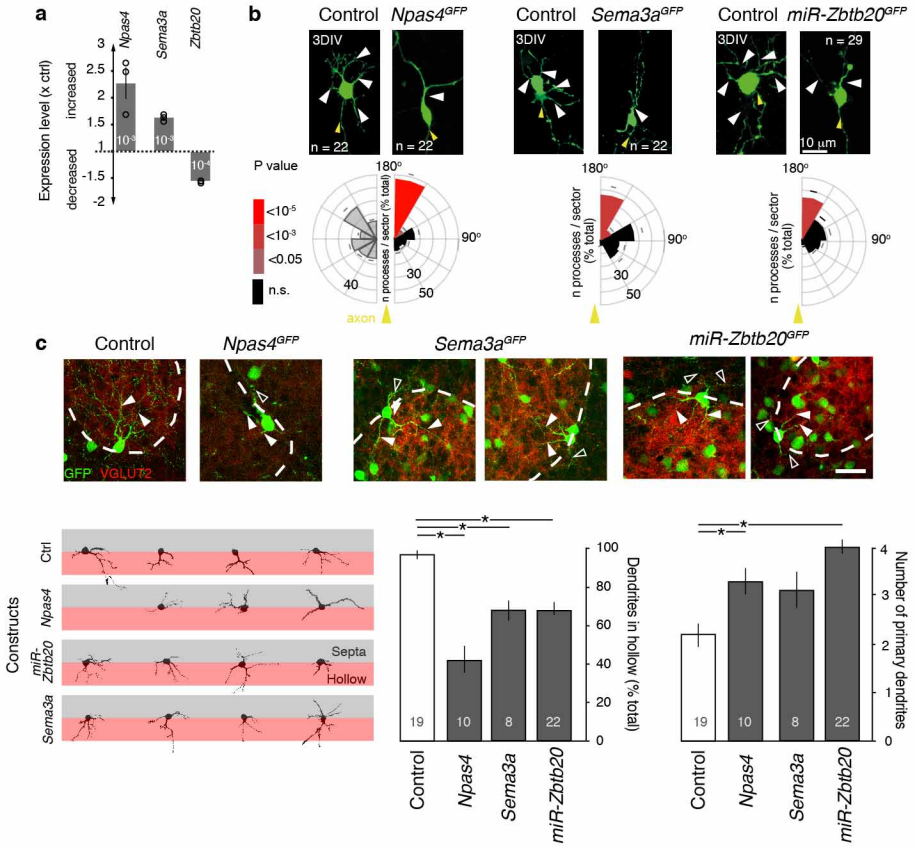

Extended Data Figure 7 | VB input regulates expression of genes controlling neurite differentiation and polarity in S1L4 neurons. **a**, *Npas4* and *Sema3a* expression is increased in vb^{-} mice, whereas *Zbtb20* is decreased. Open circles indicate values for individual replicates, value within bars indicate *P* value obtained with the microarray analysis. **b**, Overexpression of *Npas4* and *Sema3a* or downregulation of *Zbtb20* using a miR construct in S1L4 neurons collected 2 days after *in utero* electroporation at E14.5 led to changes in cell polarity. Dendrites are preferentially oriented away from the axon (yellow arrowhead, 0° in bulls eye plot), whereas they are evenly distributed when a control^{GFP} plasmid is used. *n* and *P* values are indicated in the figure, ANOVA. **c**, *In vivo* overexpression of *Npas4*, *Sema3a* or *miR-Zbtb20* by *in utero* electroporation at E14.5, the time of birth of L4 neurons, impairs dendritic orientation towards VB axons located in barrel hollows at P7 (VGLUT2^{+} region within barrels, pink area in single-cell displays) and increases in the number of primary dendrites for *Npas4* and *miR-Zbtb20* (*$P < 0.05$, ANOVA, *n* values indicated within bars). Septae correspond to spaces between barrels (grey area in single cell displays). Scale bars, 10 µm (**b**), 20 µm (**c**). See also Supplementary Note 4. Values: mean ± s.e.m.

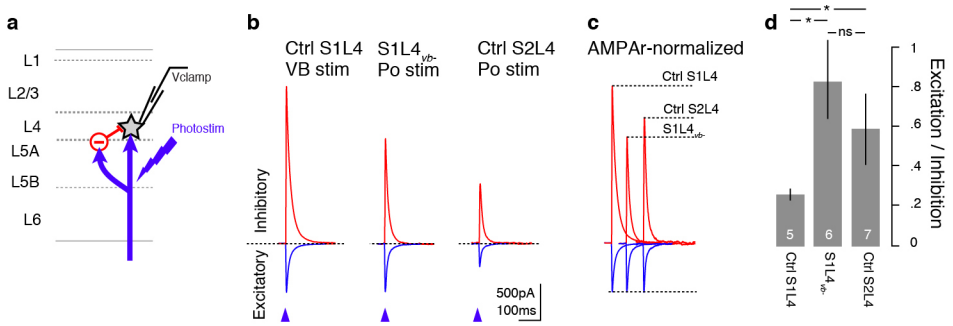

Extended Data Figure 8 | S1L4$_{vb-}$ E/I input balance is S2L4-like.
a, Schematic summary of the experiment: S1L4, S2L4 and S1L4$_{vb-}$ neurons were recorded while optogenetically stimulating the VB (for S1L4 neurons) or the Po (for S2L4 and S1L4$_{vb-}$ neurons). Feed-forward inhibitory input onto L4 neurons was determined by changing the holding potential as detailed in Methods. **b**–**d**, Sample traces (**b**) normalized to the excitatory input amplitude (**c**) and average values (**d**) showing that E/I ratios are increased to S2L4 levels in S1L4$_{vb-}$ neurons. Values: mean ± s.e.m. *$P < 0.05$, ANOVA; ns, not significant ($P = 0.4$).

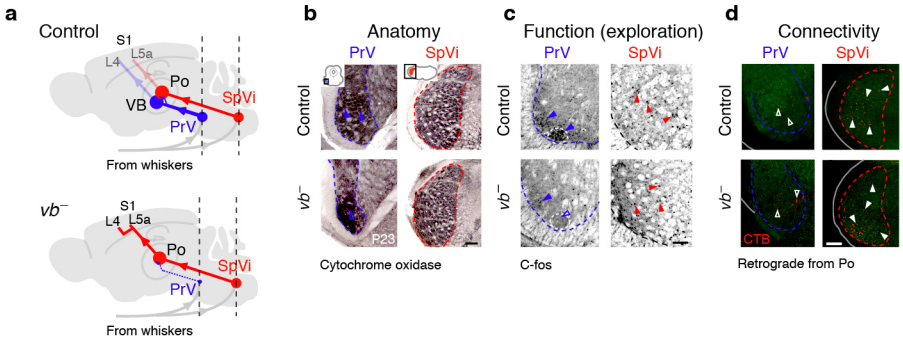

Extended Data Figure 9 | Pre-thalamic trigeminal input pathways are not rewired in *vb*⁻ mice. **a**, Schematic representation of trigeminothalamic pathways and summary of the findings. Input to the VB, which conveys information on whisker contacts, originates from the PrV nucleus of the trigeminal complex, forming the lemniscal pathway, with a small contingent of fibres reaching the VB–Po border, see Supplementary Note 6 for details). Input to the Po, which forms the paralemniscal pathway, originates from the SpVi nucleus (interpolaris part of the spinal nucleus) of the trigeminal complex. In *vb*⁻ mice, the PrV nucleus is markedly atrophied, presumably owing to loss of VB targets, and only a few cells subside. The paralemniscal pathway is unaffected. Dashed lines indicate location of the sections shown in **b**–**d**. **b**, Cytochrome oxidase staining showing markedly atrophied PrV in *vb*⁻ mice. **c**, The PrV is not detectably activated by whisker contacts during environmental exploration in *vb*⁻ mice, whereas the SpVi is unaffected. **d**, Retrograde labelling from the Po shows numerous labelled neurons in the SpVi and sparse labelled neurons in both control and *vb*⁻ mice ($n = 5$ Ctrl and $n = 3$ *vb*⁻ injections). Scale bars, 100 μm.

Extended Data Table 1 | VB input regulates a core set of genes involved in neurite differentiation and polarization

Gene symbol	Refseq ID	Fold-change (*vb* vs WT)	Function	Reference (Pubmed ID)
Nrn1	**NM_153529**	**2.93**	**extracell prot., dendritic growth**	**23115177**
NeuroD6	NM_009717	2.55	TF, axonal elongation	23303943
Nurr77	NM_010444	2.45	nuclear receptor, neurite extension	20375114
Vgf	**NM_001039385**	**2.39**	**extracell prot., dendritic growth**	**23115177**
Npas4	NM_153553	2.23	TF, neurite outgrowth	23172225
Frzb	NM_011356	2.21	extracell prot., axonal growth	16172602
Camk1g	NM_144817	2.19	prot. kinase, axonogenesis	19657032
Rorb	**NM_001043354**	**-2.17**	**nuclear receptor, adhesion**	**21799210**
N-Shc	NM_009167	2.15	TrkA receptor BP, neurite extension	12446789
Pcdh20	NM_178685	-2.02	adhesion molecule, dendritic self-avoidance	22842903
Unc5d	AK035883	-1.95	receptor, multipolar->radial polarity	22726835
Vmat2	**NM_172523**	**-1.91**	**vesicular monoamine transporter**	**12435414**
Trim67	NM_198632	-1.88	ubiquitin ligase, neuritogenesis	22337885
Rgs4	NM_009062	1.84	G-protein-binding, axonogenesis	23052218
EphA8	NM_007939	-1.80	Receptor, neurite outgrowth	15782114
Lmo4	**NM_010723**	**1.93**	**TF, Ca^{2+}-dependent**	**16899735**
Spatial	NM_001017433	-1.80	kinesin-binding prot., neurite outgrowth	24361585
Cdh18	NM_001081299	1.76	cadherin family member	17133224
Ocam	NM_001113208	1.75	membrane prot., neurite polarity	16531066
Robo3	NM_001164767	1.73	receptor, axonal guidance	18466743
ROLP	NM_183428	-1.67	adhesion molecule	19564939
Sema3a	NM_009152	1.63	extracell prot., neuronal polarization	21835341
PlxnD1	NM_026376	-1.62	Sema receptor, synaptic specificity	23395374
Cntn4	NM_001109749	1.62	membrane prot, axonal guidance	18367085
Fat3	NM_001080814	-1.59	membrane receptor, neurite pruning	21903076
Elmo1	NM_080288	1.58	spine morphogenesis	21900250
Prg5	NM_029425	1.56	membrane protein, neurite outgrowth	20032306
Cdh20	NM_011800	1.53	cadherin family member	17133224
Btbd3	**NM_145534**	**-1.52**	**TF, dendritic polarization**	**24179155**
Bhlhb5	**NM_021560**	**-1.52**	**TF, postsynaptic barrel assembly**	**18957218**
Odz3	NM_011857	-1.52	membrane prot, neuritogenesis	22367537
Zbtb20	NM_019778	-1.51	TF, cortical arealization, dendritic tufting	23283686, 19955470
Flrt3	NM_001172160	1.51	Unc5 binding prot., axonal guidance	21673655, 24560577

Genes with a demonstrated role in S1 barrel cortex formation, S1L4 neuron polarization, or TC circuit assembly appear in bold. The three genes functionally investigated in the current study are underlined. Negative values in fold-change indicate that expression is decreased in $S1L4_{vb-}$ neurons compared to control.